mathematics

Article

Combined Effects of Sequential Velocity and Variable Magnetic Field on the Phase Change Process in a 3D Cylinder Having a Conic-Shaped PCM-Packed Bed System

Lioua Kolsi [1,2], Fatih Selimefendigil [3,*], Mohamed Omri [4] and Lotfi Ladhar [5]

[1] Department of Mechanical Engineering, College of Engineering, University of Ha'il, Ha'il 81451, Saudi Arabia; lioua_enim@yahoo.fr
[2] Laboratory of Metrology and Energy Systems, Department of Energy Engineering, University of Monastir, Monastir 5000, Tunisia
[3] Department of Mechanical Engineering, Celal Bayar University, 45140 Manisa, Turkey
[4] Deanship of Scientific Research, King Abdulaziz University, Jeddah 21589, Saudi Arabia; Omrimoha2002@yahoo.fr
[5] Electrical and Computer Engineering Department, Faculty of Engineering, King Abdulaziz University, Jeddah 21589, Saudi Arabia; lladhar@kau.edu.sa
* Correspondence: fatih.selimefendigil@cbu.edu.tr; Tel.: +90-236-241-21-44; Fax: +90-236-241-21-43

Abstract: Effects of sequential velocity and variable magnetic field on the phase change during hybrid nanofluid convection through a 3D cylinder containing a phase-change material packed bed (PCM-PB) system is analyzed with the finite element method. As the heat transfer fluid, 40% ethylene glycol with hybrid TiO_2-Al_2O_3 nanoparticles is considered. Impacts of the sequential velocity parameter (K, between 0.5 and 1.5), geometric factor of the conic-shaped PCM-PB (M, between 0.2 and 0.9), magnetic field strength (Ha number between 0 and 50) and solid volume fraction of hybrid nanoparticles (vol.% between 0.02% and 0.1%) on the phase change dynamics are explored. Effects of both constant and varying magnetic fields on the phase change process were considered. Due to the increased fluid velocity at the walls, the phase change becomes higher with higher values of the sequential velocity parameter (K). There is a 21.6% reduction in phase transition time (tF) between the smallest and highest values of K both in the absence and presence of a constant magnetic field. The value of tF is reduced with higher magnetic field strength and the amount of reduction depends upon the sequential velocity parameter. At K = 1.5, the reduction amount with the highest Ha number is 14.7%, while it is 26% at K = 0.5. When nanoparticle is loaded in the base fluid, the value of tF is further reduced. In the absence of a magnetic field, the amount of phase-transition time reduction is 6.9%, while at Ha = 50, it is 11.7%. The phase change process can be controlled with varying magnetic field parameters as well. As the wave number and amplitude of the varying magnetic field are considered, significant changes in the tF are observed.

Keywords: varying magnetic field; nanofluid; phase change process; sequential velocity; FEM

Citation: Kolsi, L.; Selimefendigil, F.; Omri, M.; Ladhar, L. Combined Effects of Sequential Velocity and Variable Magnetic Field on the Phase Change Process in a 3D Cylinder Having a Conic-Shaped PCM-Packed Bed System. *Mathematics* **2021**, *9*, 3019. https://doi.org/10.3390/math9233019

Academic Editor: Marco Pedroni

Received: 18 October 2021
Accepted: 22 November 2021
Published: 25 November 2021

1. Introduction

Phase change material (PCM) applications have been considered in diverse energy related systems for thermal management and energy storage. During the recent years, the need for energy efficient products is growing due to the cost of energy and environmental concerns. The application areas for PCMs include solar power, refrigeration, thermal management in electronic devices, convective heat transfer and many others [1–3]. There is a need for increasing the effectiveness of using PCMs and many different methods have been offered. They are used with highly conductive fins, metal foams and nano-sized particles [4–9]. PCM-packed bed (PB) systems are also used in applications, such as in air conditioning, building, solar and many others, as they offer many advantageous [10].

Different applications of PCM-PB system with existing numerical models and available correlations have been reviewed in the work of [11]. The external flow conditions and geometric modification in the container with PCM-installed systems can also be considered as potential methods for increasing the effectiveness of PCM-PB systems. The velocity profile at the inlet section may be used to control the phase change (PC) process in the PCM-installed systems. Pulsating flow has been used in diverse applications for convective heat transfer (HT) control. Theoretical [12], experimental [13,14] and numerical studies [15–17] have been performed to show the impacts of flow pulsation and its parameters of the fluid flow and HT characteristics. In a PCM-PB system, the velocity profile at the inlet can be made non-uniform and the wall region velocity can be varied by using a sequential velocity. The wall region velocity may be different from the interior domain velocity where PC is expected to be fast. This will have impacts on the PC process near the walls. On the other hand, the shape of the container where PCM is installed can also be varied. This will affect the flow dynamics within the PCM region and number of encapsulated spheres. Therefore, the phase transition time will be controlled. In this study, the PCM zone has a conic shape and the geometric controlling parameter is the ratio of the conic base radius.

In another method for controlling the PC process dynamics, the magnetic field (MF) can be used. These effects are relevant in many engineering applications, such as in micro-pumps, glass float, coolers of nuclear reactor, geothermal energy and many different systems [18–20]. In convective HT applications, an external MF can be used for controlling the flow features and thermal performance improvements [21–24]. The effectiveness of using MF can be further improved by using nano-sized particles in the HT fluid [25–27]. Some aspects such as non-Newtonian fluid behavior under MF effects have been studied in [28–33].

Thermophysical properties including electrical and thermal conductivity will be altered by using nano-sized particles. The technology of nanofluid has been implemented in diverse energy systems, including solar power, refrigeration, electronic cooling and many different areas [34–37]. In thermal energy storage, nano-sized particles have also been used [38–41]. In applications with PCM-PB systems, the utilization of MF effects have the potential to increase the PC process, especially near the wall regions. The utilization of nano-sized particles in the HT fluid increases the electrical conductivity and effectiveness of MF becomes more apparent. It also improves the thermal transport within the PCM-installed zone while the phase transition is expected to be accelerated. The utilization of MF effects and nanofluid for the PC process have been considered in several works [42–47].

In the present work, the MF effects will be used with nanofluid for PCM-PB system considering the spatially varying MF. The uniform and non-uniform MF effects have different impacts on the fluid flow and HT dynamics, as it has been shown in many convective HT studies [48–50].

In this study, PC dynamics in a PCM-PB system is analyzed under spatially varying MF and nanoparticle loading in the base fluid. A novel method of controlling the inlet velocity of the HT fluid by using a sequential approach is adopted. The advantages of the approach are that, it allows to vary the velocity near the wall regions and to control the PC process in the vicinity of this zone. By combining the spatially varying MF effects and sequential velocity parameters, the PC process will be improved while further performance improvements will be achieved by using nano-sized particles in the base fluid. As diverse applications exist for the utilization of the PCM-PB system, the proposed methods will be helpful in the design, optimization, development of new systems and related thermal energy storage technologies.

2. Mathematical Formulation

A cylindrical reactor with an embedded PCM-PB system is analyzed during nanofluid convection under MF effects as shown in Figure 1. The PCM is contained in a conic-shaped region with heights of h1 and h2, while the aspect ratio is defined as M = h1/h2. The spherical-shaped encapsulated PCM is considered with a particle size of 20 mm. At the inlet section, a sequential velocity is defined. For half of the inlet, it is uniform with a value of u1 while for the other half of the section, it is u0. The sequential velocity parameter is described with K = u1/u0. This shows the significance of the velocity near the wall region which is important to be considered for the PC process. The fluid temperature at the inlet is Ti. The distance of the PCM-PB region from the inlet is H1, while H2 is the distance from the exit. The radius of the cylindrical reactor is L = 2L0, while H is the height. A radially acting MF is imposed within the whole computational domain. Constant and spatially varying MF effects are used. In the case of spatially varying MF, a sinusoidal form with wave number (N) and amplitude of A is considered as shown in Figure 2.

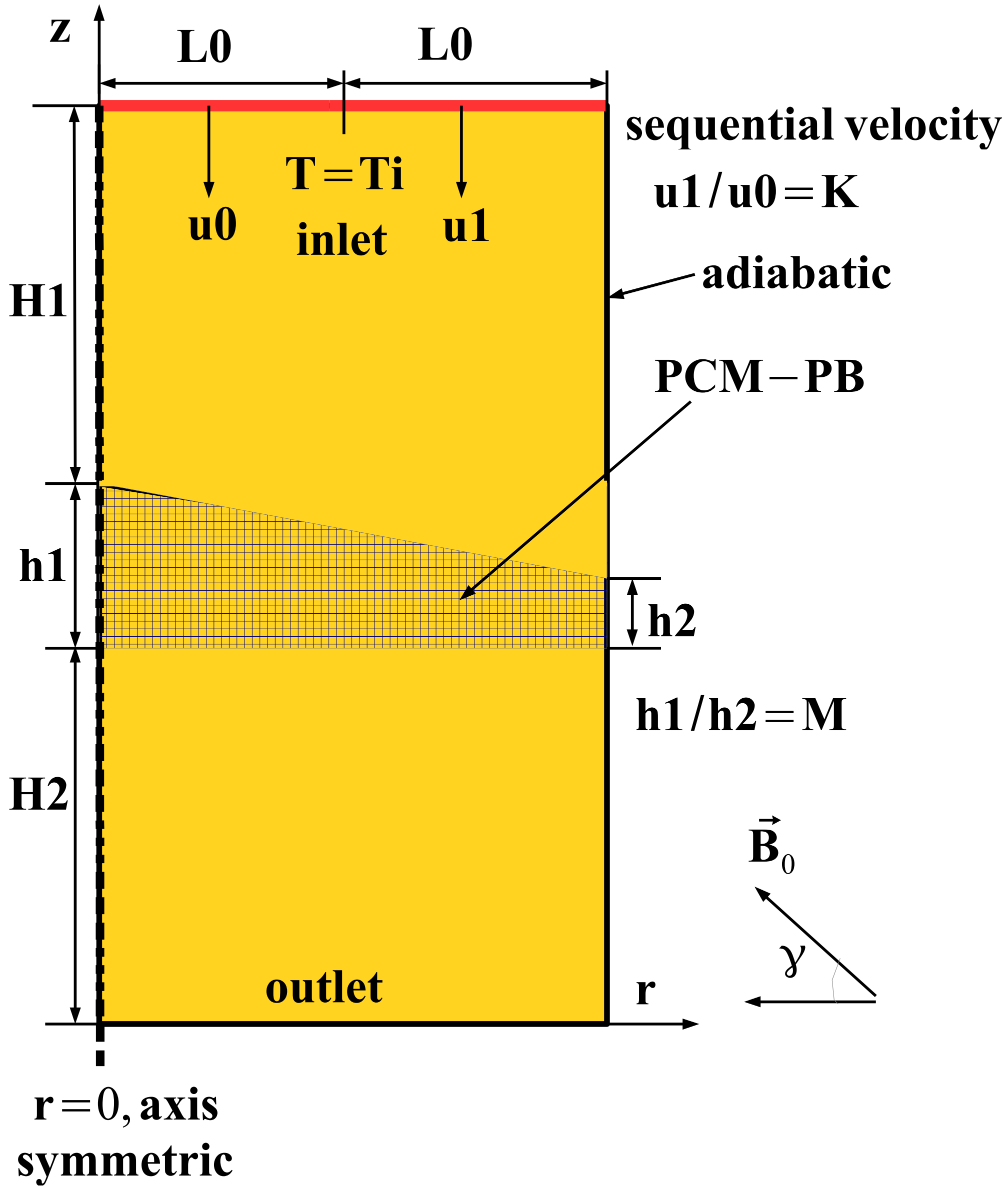

Figure 1. Schematic view of the geometry with boundary conditions.

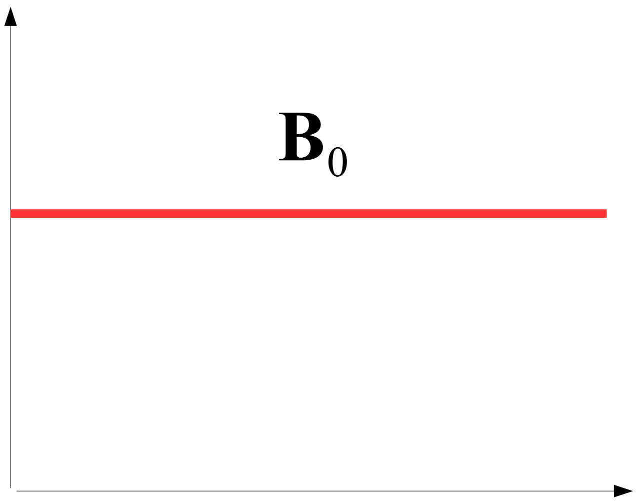

(**a**) constant MF

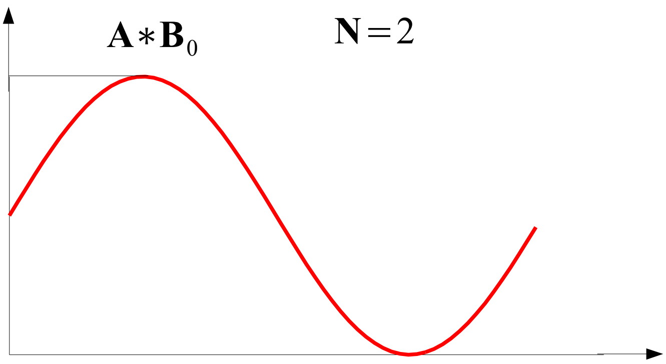

(**b**) variable MF, N = 2

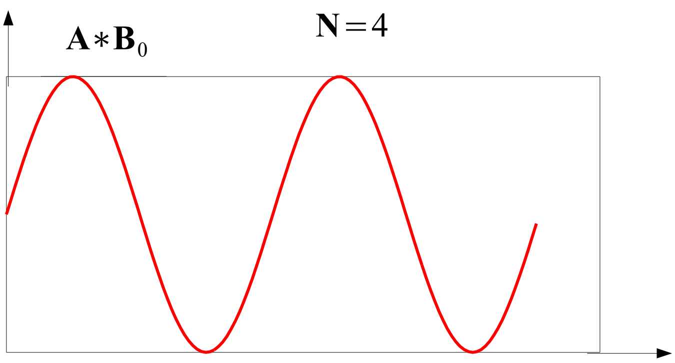

(**c**) variable MF, N = 4

Figure 2. Configurations for constant MF (**a**) and variable MF (**b**,**c**).

Hybrid TiO_2-Al_2O_3 nanoparticles are used in the 40% ethylene glycol [51] which is used as the HT fluid. The nanofluid shows Newtonian behavior and the effective thermal conductivity (k_{nf})/viscosity (μ_{nf}) property equations were derived by using experimental data. They are given with the following expressions [51]:

$$k_{nf} = 0.386e^{(2.27\phi+0.002939T)}, \tag{1}$$

$$\mu_{nf} = 7.1074 + 3.65\phi - 0.14097T + 0.05176\phi T + 0.907\phi\phi + 0.00092T^2. \quad (2)$$

The above given correlations are valid for 30–80 °C and 0.02–0.1%. In this range, the nanofluid is also shown to behave as Newtonian. Effects of thermal radiation, Joule heating, induced MF and displacement currents are ignored during the simulation. The conservation equations in general form can be written as:

$$\nabla.\mathbf{u} = \mathbf{0} \quad (3)$$

$$\begin{aligned} \delta_1 \tfrac{1}{\varepsilon_p^2}\rho(\mathbf{u}.\nabla)\mathbf{u} = \quad & \nabla.\left[-p\mathbf{I} + \tfrac{\delta_2}{\varepsilon_p}\mu\left(\nabla\mathbf{u} + (\nabla\mathbf{u})^T\right)\right] \\ & -\delta_3\left(\mu\kappa^{-1} + \beta_p\rho|\mathbf{u}|\right)\mathbf{u} + \vec{F}_M \end{aligned} \quad (4)$$

$$\rho C_p \frac{\partial T}{\partial t} + \rho C_p \mathbf{u}.\nabla T = \nabla.(k\nabla T), \quad (5)$$

where Kozeny–Carmen permeability model is utilized:

$$\kappa = \frac{d_p^2}{180}\frac{\varepsilon_p^3}{(1-\varepsilon_p)^2} \quad (6)$$

In the above equations, the values of $\delta_1, \delta_2, \delta_3$ become 1 for the PCM region, while they are $\varepsilon_p^2, \varepsilon, 0$ for the nanofluid region outside PCM. Lorentz forces due to the external MF are included in the equations while it is acting in the radial direction as:

$$F_{M,r} = 0, \;\; F_{M,z} = -\sigma w B_{0r}^2. \quad (7)$$

For the PCM zone, a function α is used which has values of 0 $(T < (T_m - \Delta T_m/2))$ and 1 $(T > (T_m + \Delta T_m/2))$. The energy equation with the following properties is used:

$$\begin{aligned} & c_p = \frac{1}{\rho}\left(\theta\rho_{p1}c_{p,p1} + (1-\theta)\rho_{p2}c_{p,p2}\right) + L\frac{\partial\alpha_m}{\partial T}, \\ & k = \theta k_{p1} + (1-\theta)k_{p2}, \;\; \alpha_m = \frac{1}{2}\frac{(1-\theta)\rho_{p2} - \theta\rho_{p1}}{\theta\rho_{p1} + (1-\theta)\rho_{p2}}, \\ & \theta = 1-\alpha, \;\; \rho = \theta\rho_{p1} + (1-\theta)\rho_{p2}. \end{aligned} \quad (8)$$

The phases are given with $p1$ and $p2$ while L denotes the latent heat of fusion. Between the phases, a non-equilibrium HT interface is utilized, while phases and source terms equations are stated as in the following.

A non-equilibrium H-T interface is used between the phases. Equations for phases and source terms are given as [52,53]:

$$\mathbf{q_s} = -\theta_p k_s \nabla T_s, \;\; \mathbf{q_f} = -(1-\theta_p)k_f \nabla T_f. \quad (9)$$

$$\theta_p \rho_s C_{p,s}\frac{T_s}{\partial t} + \nabla.\mathbf{q_s} = q_{sf}\left(T_f - T_s\right) + \theta_p Q_s, \quad (10)$$

The terms $\mathbf{q_f}$ and $\mathbf{q_s}$ denote the conductive heat fluxes of phases, while q_{sf} and Q are the interstitial convective HT and source term. The related HT coefficient is described with the following equation [52,53]:

$$\frac{1}{h_{sf}} = \frac{2r_p}{k_f \mathrm{Nu}} + \frac{2r_p}{\beta k_s}. \quad (11)$$

The β value is 10 for spherical particles while the fluid-to-solid Nu number is written as [54]:

$$\mathrm{Nu} = 2 + 1.1\mathrm{Pr}^{1/3}\mathrm{Re}_p^{0.6}. \quad (12)$$

The particle Prandtl number (Pr) and Reynolds number (Re) are described by the following:

$$\mathrm{Pr} = \frac{\mu c_{p,f}}{k_f}, \quad \mathrm{Re}_p = \frac{2r_p \rho_f |u_f|}{\mu}. \tag{13}$$

The inlet temperature of the nanofluid is taken as Ti = 345 K. The inlet temperature is sequential and it has values of u1 and u0. A sequential velocity parameter K is defined as K = u1/u0. The inlet temperatures near the wall and interior domain region can be varied which can be used to control the PC process. An axis-symmetrical model is used ($\frac{\partial T}{\partial n} = 0$). The walls of the cylindrical container are adiabatic while a pressure outlet is used at the exit. The value of the initial temperature is taken as 303 K. The PCM zone is included in a conic-shaped region with an aspect ratio of M = h1/h2 and it is also varied during the simulation. Both constant and spatially varying MF effects are considered. A sinusoidal-shaped spatially varying MF is considered while the impacts of wave amplitude and its number on the PC process are examined.

The Reynolds number (Re) and Hartmann number (Ha) are the relevant non-dimensional numbers and they are described as:

$$\mathrm{Re} = \frac{\bar{u} H \rho}{\mu}, \quad \mathrm{Ha} = B_0 H \sqrt{\frac{\sigma}{\rho \nu}}. \tag{14}$$

where $\bar{u}$ is the average velocity at the inlet section.

The solution of the above given equations is made by using a Galerkin weighted residual Finite Element Method (FEM). Approximated field variables of interest are used in the governing equations. The approximation is stated as in the following:

$$b = \sum_{k=1}^{N^s} \Phi_k^s B_k \tag{15}$$

where Lagrange finite elements of different orders are used for the approximation of any field variable of interest (b). Φ^s and B_k denote the shape function and nodal value. The weighted average of the residuals (R) is set to be zero as by using a wright function (W) as in the following:

$$\int_V WRdV = 0. \tag{16}$$

The following convergence criteria is considered:

$$\left| \frac{\Gamma^{n+1} - \Gamma^n}{\Gamma^{n+1}} \right| \leq \eta \tag{17}$$

where n denotes the iteration number. The convergence criterion of $\eta = 10^{-7}$ is set. The time-dependent part is treated by using a second-order backward differentiation (BFD) algorithm. The commercial computational fluid dynamics (CFD) code Comsol [53] is utilized.

Grid independence is tested by using different number of elements. Figure 3a shows the full phase transition times (tF in minutes) for various grid sizes at two MF strengths. Grid system G5 with 56,892 number of elements is selected for the subsequent computations. The grid is refined at the interfaces and towards the walls. The grid distribution of the computational model is given in Figure 3b.

For the validation purpose, two different studies are used. In the first work, convective HT in a differentially heated cavity under MF effects is considered as in the study available in [55]. Comparisons of the average Nu with different Ra numbers at Ha = 30 are shown in Figure 4. The highest deviation below 3% between the results is obtained. In the second validation study, results from [56] were used where PC dynamics in a differentially heated cavity were examined. Comparisons of the solidified volume fraction which depends upon the dimensionless time (t_1), aspect ratio (Ar) and Rayleigh number (Ra) are shown in Figure 5. The maximum deviation of −9.3% is observed.

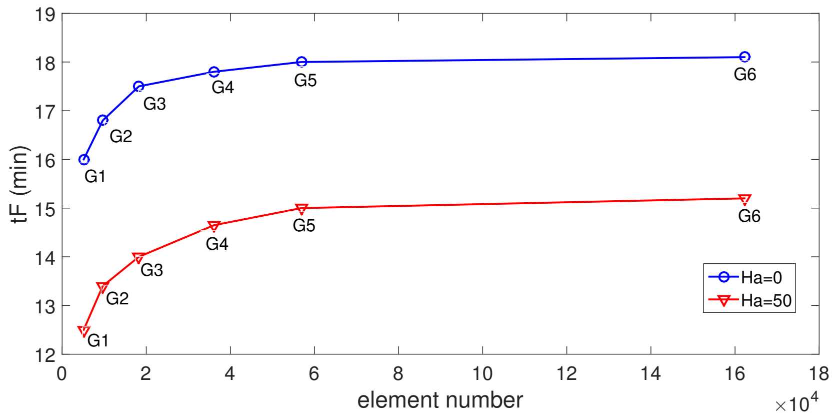

(**a**)

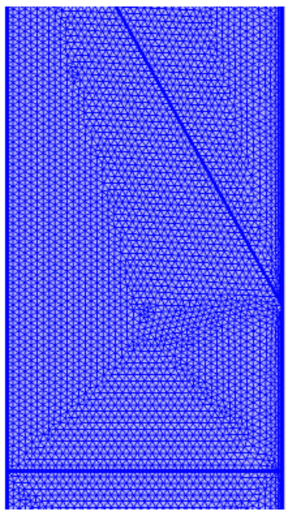

(**b**)

Figure 3. Grid-independence test results for various grid sizes at two different MF strengths (**a**) and grid distributions of the model (**b**) (constant MF, $M = 0.5$, $\phi = 0.1\%$).

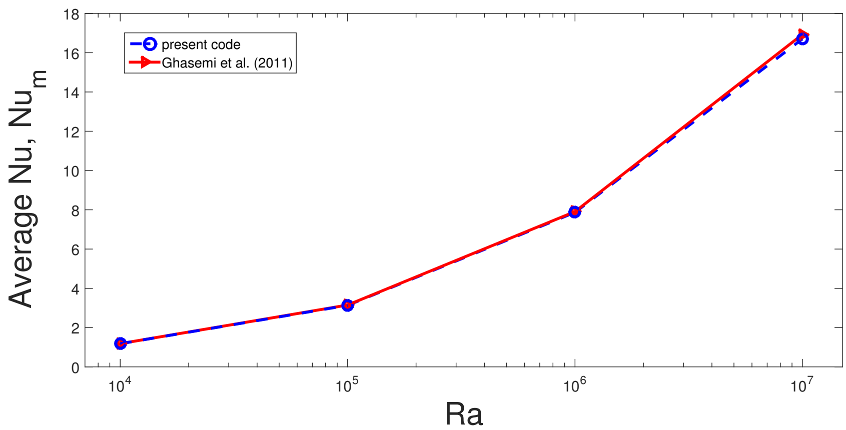

Figure 4. Code validation 1: comparisons of the average Nu for different Rayleigh numbers at a Hartmann number of 30. Results presented in [55] were used.

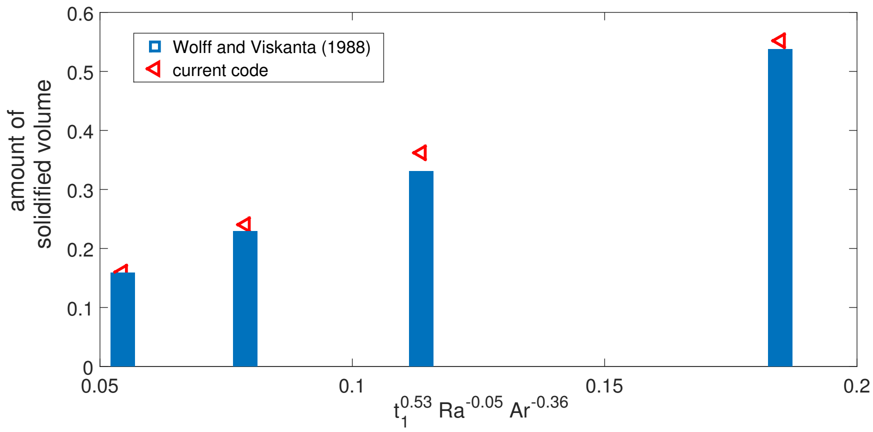

Figure 5. Code validation 2: comparisons of the solidified volume fraction for PC dynamics in a differentially heated cavity. Results presented in [56] were used.

3. Results and Discussion

Combined impacts of using sequential velocity and variable MF on the PC during hybrid nanofluid convection through a 3D cylinder containing PCM-PB system is analyzed with FEM. Impacts of sequential velocity parameter (K, between 0.5 and 1.5), conic shape PCM-PB geometric factor (M, between 0.2 and 0.9), strength of MF (Ha number between 0 and 50) and solid volume fraction of hybrid nanoparticles (between 0.02% and 0.1%) on the PC dynamics are numerically assessed.

The sequential velocity parameter (K) is used to define different velocity levels near the walls and in the interior domain. Phase completion time is slow especially near the walls which needs to be accelerated. Impacts of the sequential parameter (K) on the time evolution of the liquid fraction (LFR) are shown in Figure 6. A higher value of K denotes a higher velocity component near the wall of the inlet section. At higher times, phase change (PC) accelerated especially in the interior domain. As the value of K is increased, it becomes fast in those regions as well and, at t = 16 min for K = 1.5, full phase completion is observed. The dynamics of the PC process is represented in terms of average liquid fraction (LFR) and it is affected by the variation of K. A higher value of K results in a fast PC process and a reduction of the full phase transition time (tF in minutes) is seen (Figure 7a,b).

This feature is observed either in the absence (Ha = 0) or presence of MF effects (Ha = 50). In the absence of MF effects, the amount of reduction in tF is 32%, while this is 22% when cases with the smallest and largest K values are compared. This shows that the MF effects also become important when sequential velocities are considered at the inlet section. Figure 8 shows the impacts of MF strength on the distribution of the time-dependent liquid fraction. At higher times, the effects of using MF become apparent as the LFR becomes higher near the walls. This is due to the enhanced effects of velocity near the walls with higher MF while thermal transport is increased and the PC process is accelerated. This will even become faster by increasing the sequential parameter (K) as shown in Figure 8, where full phase completion is achieved at t = 16 min. The characteristics of the dynamics for LFR with varying MF strengths depend upon the sequential parameter. As the value is lower which indicates lower fluid velocities near the wall, the MF has positive impacts at later times. As the MF strength is increased, the PC process is accelerated while a reduction in the complete phase transition time is achieved (Figure 9c). The impacts of MF on the PC is more pronounced, especially when the value of K is small where the fluid velocity near the wall becomes smaller. At K = 0.5, the amount of reduction in tF is 26% when cases with MF at Ha = 0 and Ha = 50 are compared. However, this value becomes only 14.7% when configurations at K = 1.5 are considered.

Including nano-sized particles in the base fluid improves the thermal transport and the PC process is expected to be fast. The dynamic features of the LFR are influenced by including nanoparticles and increasing their amount in the HT fluid as shown in Figure 10a,b. A reduction in the full phase transition time (tF) is seen with higher solid volume fraction (svf). The amount of reduction in tF also depends upon the MF strength. In the absence of MF effects, there is 7% reduction in tF with the highest svf of nanoparticles loading, while this is 12% when MF at the highest strength (Ha = 50) is considered. When nanoparticles are used, both thermal and electrical conductivities are enhanced. As the MF has positive impacts on the PC process due to the increased fluid velocity near the walls, increasing the svf of nanoparticles in the fluid, further improves the performance of PC under MF effects with higher strengths.

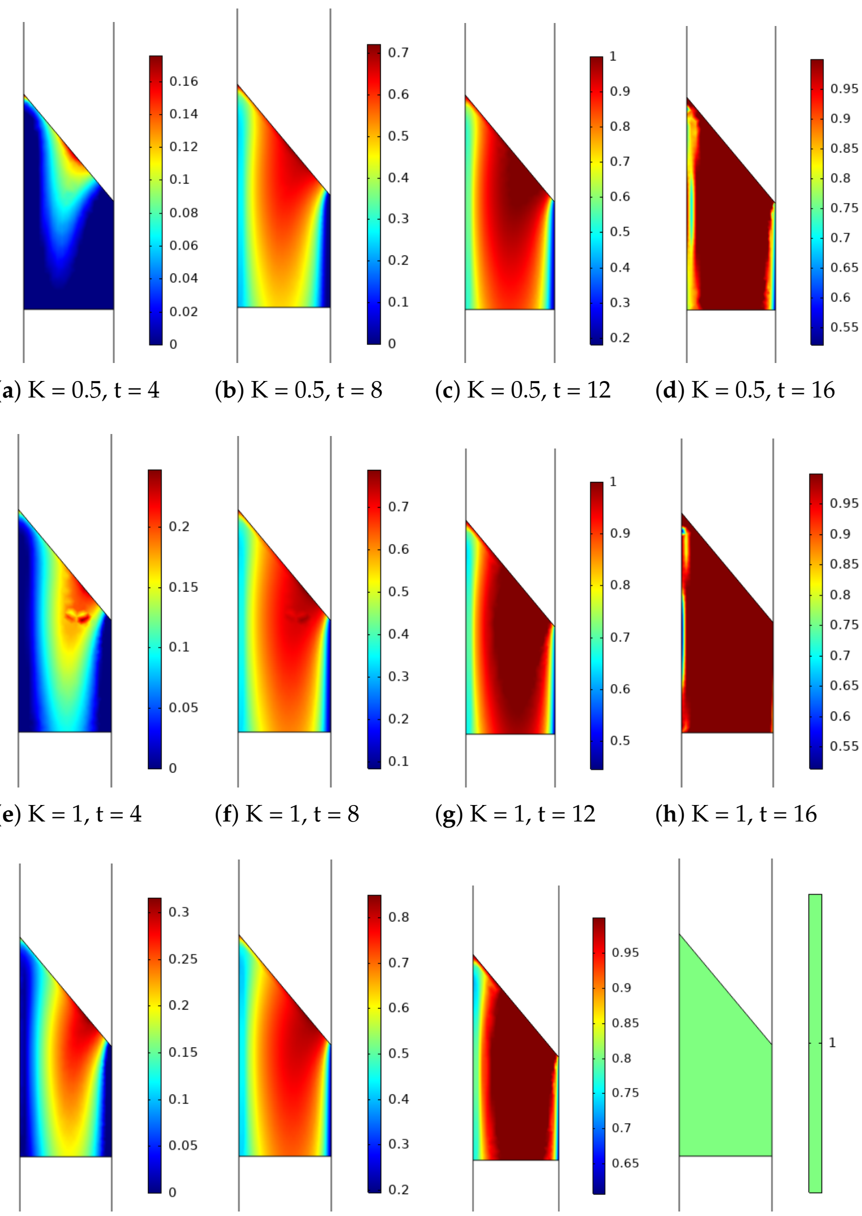

(**a**) K = 0.5, t = 4 (**b**) K = 0.5, t = 8 (**c**) K = 0.5, t = 12 (**d**) K = 0.5, t = 16

(**e**) K = 1, t = 4 (**f**) K = 1, t = 8 (**g**) K = 1, t = 12 (**h**) K = 1, t = 16

(**i**) K = 1.5, t = 4 (**j**) K = 1.5, t = 8 (**k**) K = 1.5, t = 12 (**l**) K = 1.5, t = 16

Figure 6. Effects of the sequential velocity parameter (K) on the distribution of liquid fraction (LFR) at various time instances (t in minutes) (**a**–**l**) (constant MF, Ha = 15, $M = 0.5$, $\phi = 0.1\%$).

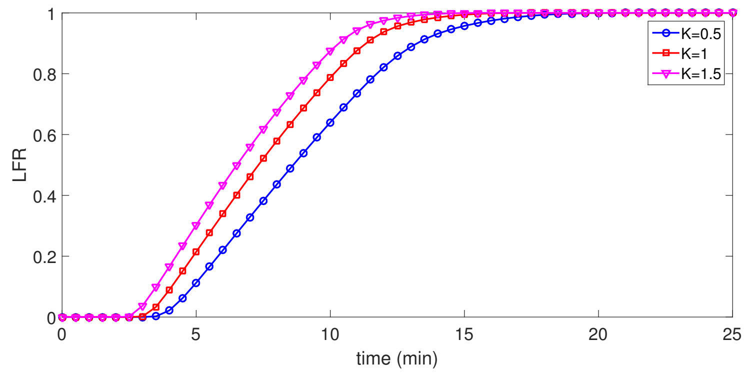

(**a**) Ha = 15, M = 0.5

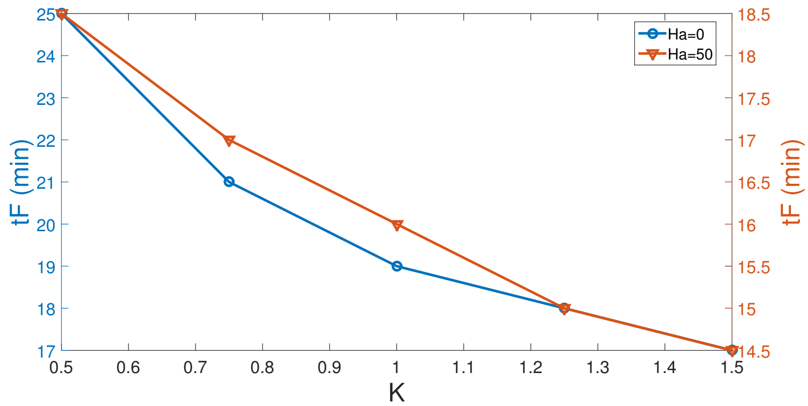

(**b**) M = 0.5

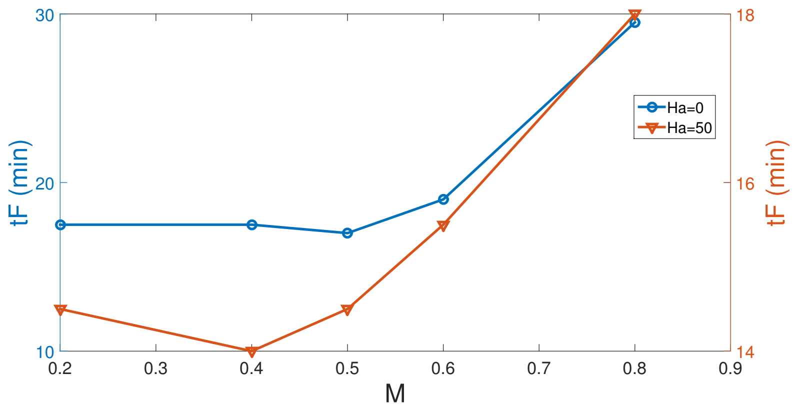

(**c**) K = 1.5

Figure 7. Impacts of the sequential velocity parameter (K) on the time evolution of the liquid fraction (LFR) (**a**) and complete phase transition time (**b**); effects of the conic aspect ratio (M) on the time-dependent variation of phase completion time (**c**). In case (**b**,**c**), left and right y-axes show results for Ha = 0 and Ha = 50 (constant MF, $\phi = 0.1\%$).

The MF can be constant as discussed above or it may be imposed as spatially varying. We considered a sinusoidal shape in the radial direction for the MF strength. Its amplitude is A and the number of waves denote the number of half sinus waves which is represented by N. For comparisons, the constant magnetic field case is also considered for the PC process. Figure 11 shows the complete phase transition time (tF) with varying amplitude (A), wave number (b) and strength (c) of the spatially varying MF. When the amplitude of spatially varying MF increases, the value of tF reduces which is due to the increased effects of MF within the domain. There is 11% variation in the value of tF for configurations with the smallest (A = 0.1) and largest (A = 1) amplitudes. The values of tF first reduces from N = 1 to N = 2 and, then, increases thereafter from N = 2 to N = 12. There is 16% variation in the phase completion time when the wave number of the spatially varying MF is altered. Both in the cases with constant MF and variable MF effects, the phase change process becomes fast with higher MF strengths. The case of constant MF resulted in fast transition times as it is expected due to the effectiveness of the MF within the PCM region. The reduction amount of tF is 18% for the case of constant MF at the highest strength, while this is only 11% for the varying MF case at Ha = 50.

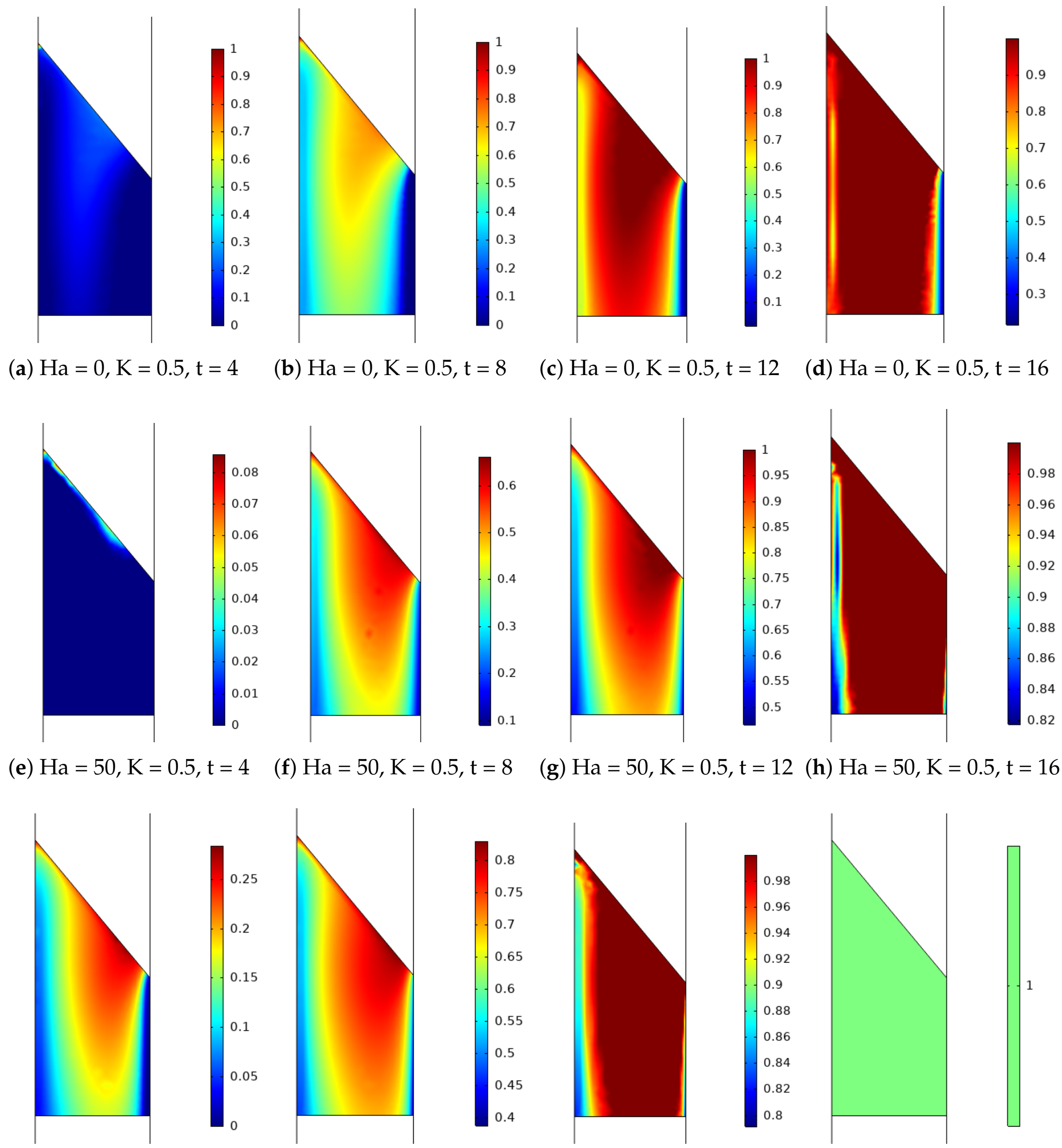

(**a**) Ha = 0, K = 0.5, t = 4 (**b**) Ha = 0, K = 0.5, t = 8 (**c**) Ha = 0, K = 0.5, t = 12 (**d**) Ha = 0, K = 0.5, t = 16

(**e**) Ha = 50, K = 0.5, t = 4 (**f**) Ha = 50, K = 0.5, t = 8 (**g**) Ha = 50, K = 0.5, t = 12 (**h**) Ha = 50, K = 0.5, t = 16

(**i**) Ha = 50, K = 1.5, t = 4 (**j**) Ha = 50, K = 1.5, t = 8 (**k**) Ha = 50, K = 1.5, t = 12 (**l**) Ha = 50, K = 1.5, t = 16

Figure 8. Time evolution of liquid fraction (LFR) distribution for (Ha = 0, K = 0.5) (**a**–**d**), for (Ha = 50, K = 0.5) (**e**–**h**) and for (Ha = 50, K = 1.5) (**i**–**l**) (constant MF, $M = 0.5$, $\phi = 0.1\%$).

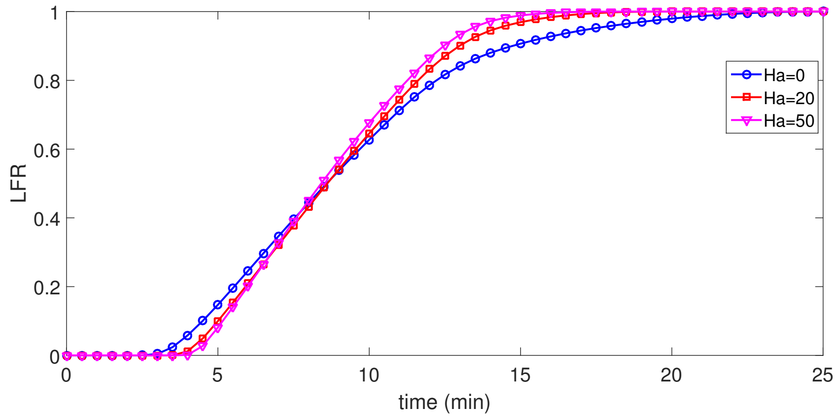

(**a**) K = 0.5

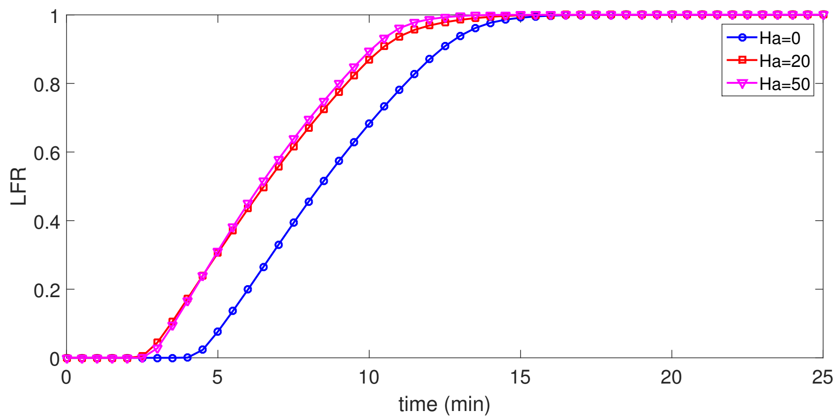

(**b**) K = 1.5

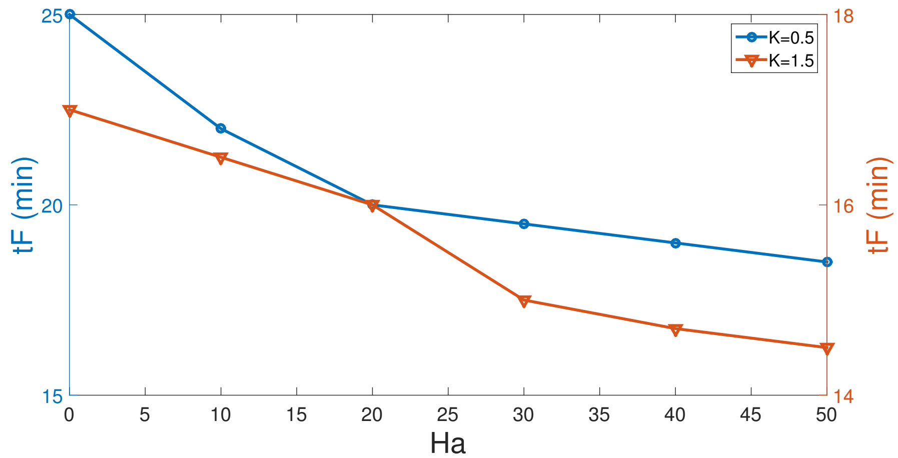

(**c**)

Figure 9. Impacts of MF strength on the dynamic features of the LFR at K = 0.5 (**a**), K = 1.5 (**b**) and on the complete phase transition time (**c**). In case (**c**), left and right y-axes show results for K = 0.5 and K = 1.5 (constant MF, $M = 0.5,\ \phi = 0.1\%$).

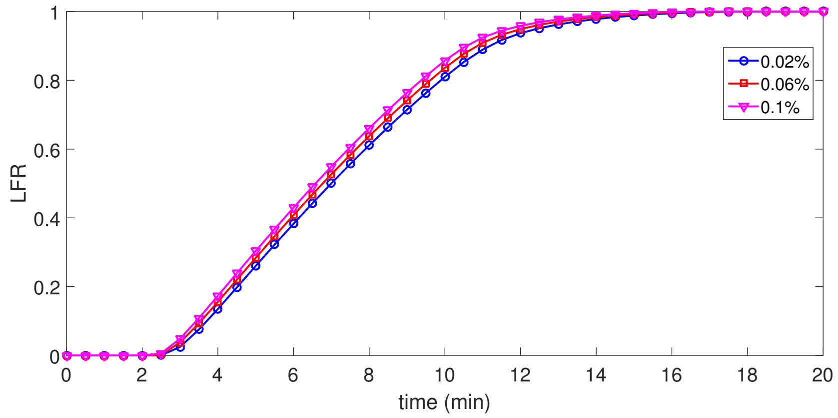

(**a**) Ha = 0

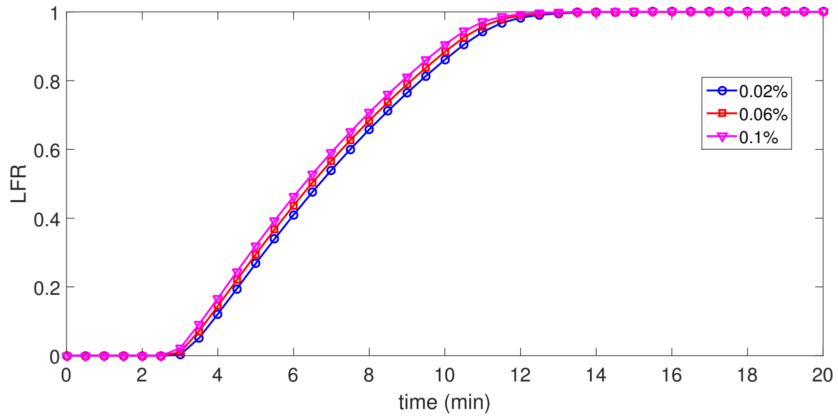

(**b**) Ha = 50

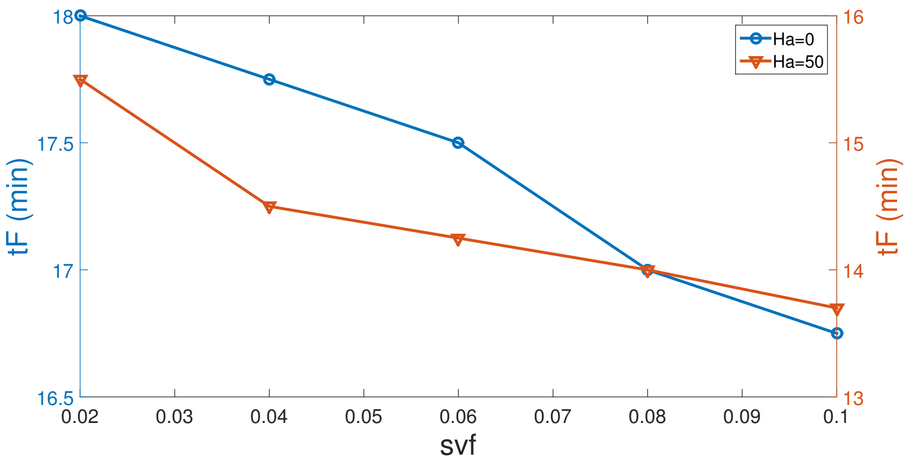

(**c**)

Figure 10. Solid volume fraction (svf) of nanoparticles on the time-dependent variation of LFR at Ha = 0 (**a**), at Ha = 50 (**b**) and on the phase completion time (**c**). In case (**c**), left and right y-axes show results for Ha = 0 and Ha = 50 (constant MF, $K = 1.5$, $M = 0.5$).

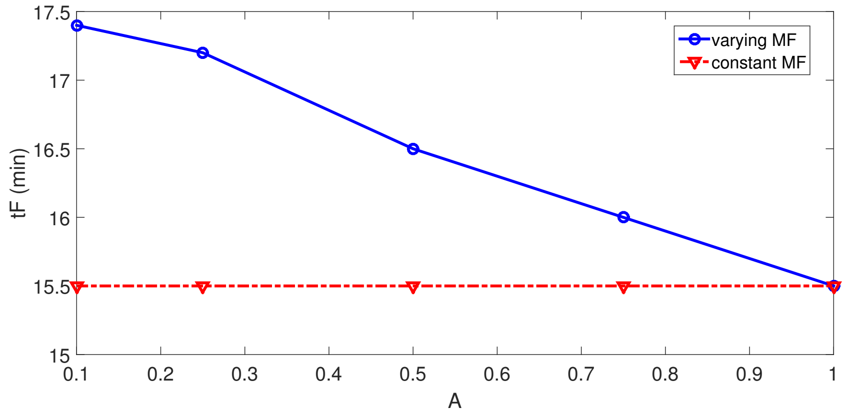

(**a**) N = 3, Ha = 40

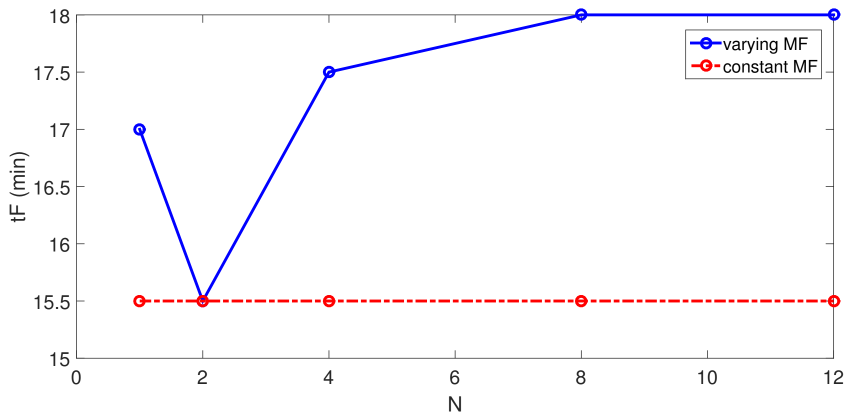

(**b**) A = 0.5, Ha = 40

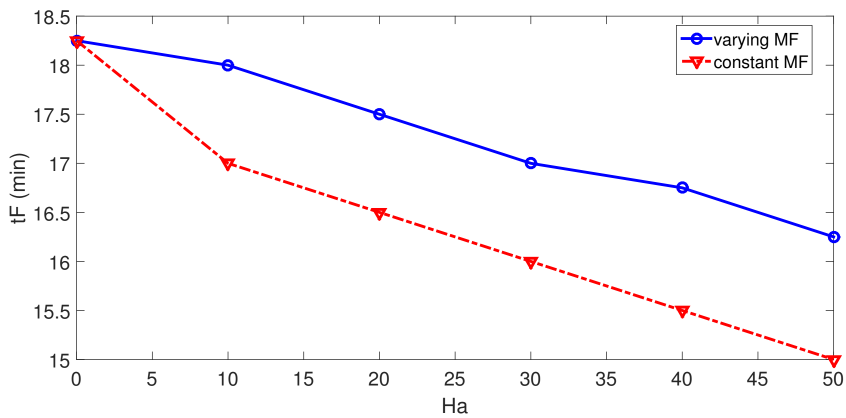

(**c**) A = 0.5, N = 3

Figure 11. Impacts of varying MF amplitude (**a**), wave number (**b**) and MF strength (**c**) on the variation of the complete phase transition time ($K = 1.25, M = 0.5, \phi = 0.1\%$).

4. Conclusions

A novel technique for fast phase transition and control is proposed for a PCM-PB system with a 3D cylinder during hybrid nanofluid convection by using sequential velocity and variable MF effects. The following conclusions can be drawn:

- As the sequential velocity parameter (K) becomes higher, a fast phase transition occurs due to the enhanced wall region velocity. When cases with the lowest and highest K are compared, there is 21.6% reduction in the complete phase transition time (tF).
- Higher MF strength resulted in fast PC. The impact of MF on the PC process is significant with lower values of K while at K = 0.5, tF is reduced by about 26% at the highest MF strength.
- Nanoparticle utilization in the base fluid further improves the performance. This is more effective in the presence of MF effects at the highest strength while 12% reduction in the tF is obtained at the highest nanoparticle concentration.
- When spatially varying MF effects are considered, a 11% variation in the phase completion time is observed when the cases with the largest and smallest wave amplitudes are compared.
- When the wave number of the spatially varying MF effects are considered, 16% variation in the tF is seen for the cases with the largest and smallest wave numbers.
- Sequential velocity and MF combination provides a novel way of controlling the PC process with with the 3D cylindrical reactor with an installed PCM-PB system.

The present study shows that using sequential velocity and MF together, the PC dynamics can be controlled effectively. As PCM-installed systems are relevant in many technological applications ranging from thermal energy storage to thermal management in solar energy, electronic cooling, waste heat recovery, heat exchanger design and many others, the outcomes of the present work can be used for the design and optimization of the PC process in diverse applications. The current work can be extended to include different nanoparticles, shape effects of nanoparticles, different PCMs and different thermal boundary conditions.

Author Contributions: Conceptualization, F.S.; methodology, F.S., L.K. and M.O.; software, F.S.; validation, L.K.; formal analysis, F.S. and L.K.; investigation, F.S., L.K., M.O.; writing—original draft preparation, F.S.; writing—review and editing, F.S., L.K., M.O. and L.L.; visualization, F.S. and L.K.; supervision, F.S., L.K., M.O. and L.L. All authors have read and agreed to the published version of the manuscript.

Funding: This project was funded by the Deanship of Scientific Research (DSR), King Abdulaziz University, Jeddah, Saudi Arabia, under grant No. (D-229-135-1442). The authors, therefore, gratefully acknowledge DSR technical and financial support.

Institutional Review Board Statement: Not applicable.

Informed Consent Statement: Not applicable.

Conflicts of Interest: The authors declare no conflict of interest.

Abbreviations

A	wave amplitude
h	heat transfer coefficient, (W/m^{2}K)
H	reactor height, (m)
Ha	Hartmann number
k	thermal conductivity, (W/mK)
K	sequential velocity parameter
M	geometric factor
N	wave number
Nu	Nusselt number
p	pressure, (Pa)
Pr	Prandtl number
Re	Reynolds number
T	temperature, (K)
u, v	x-y velocity components, (m/s)
x, y	Cartesian coordinates, (m)

Greek Characters	
α	thermal diffusivity, (m^2/s)
ϕ	solid volume fraction
ν	kinematic viscosity, (m^2/s)
ρ	density of the fluid, (kg/m^3)
Subscripts	
c	cold
h	hot
m	average
nf	nanofluid
p	solid particle

References

1. Kasaeian, A.; Bahrami, L.; Pourfayaz, F.; Khodabandeh, E.; Yan, W.M. Experimental studies on the applications of PCMs and nano-PCMs in buildings: A critical review. *Energy Build.* **2017**, *154*, 96–112. [CrossRef]
2. Sheikholeslami, M.; Mahian, O. Enhancement of PCM solidification using inorganic nanoparticles and an external magnetic field with application in energy storage systems. *J. Clean. Prod.* **2019**, *215*, 963–977. [CrossRef]
3. Shalaby, S.; Bek, M.; El-Sebaii, A. Solar dryers with PCM as energy storage medium: A review. *Renew. Sustain. Energy Rev.* **2014**, *33*, 110–116. [CrossRef]
4. Hosseinizadeh, S.; Tan, F.; Moosania, S. Experimental and numerical studies on performance of PCM-based heat sink with different configurations of internal fins. *Appl. Therm. Eng.* **2011**, *31*, 3827–3838. [CrossRef]
5. Khanna, S.; Reddy, K.; Mallick, T.K. Optimization of finned solar photovoltaic phase change material (finned pv pcm) system. *Int. J. Therm. Sci.* **2018**, *130*, 313–322. [CrossRef]
6. Mat, S.; Al-Abidi, A.A.; Sopian, K.; Sulaiman, M.Y.; Mohammad, A.T. Enhance heat transfer for PCM melting in triplex tube with internal–external fins. *Energy Convers. Manag.* **2013**, *74*, 223–236. [CrossRef]
7. Heyhat, M.M.; Mousavi, S.; Siavashi, M. Battery thermal management with thermal energy storage composites of PCM, metal foam, fin and nanoparticle. *J. Energy Storage* **2020**, *28*, 101235. [CrossRef]
8. Deng, Z.; Liu, X.; Zhang, C.; Huang, Y.; Chen, Y. Melting behaviors of PCM in porous metal foam characterized by fractal geometry. *Int. J. Heat Mass Transf.* **2017**, *113*, 1031–1042. [CrossRef]
9. Tariq, S.L.; Ali, H.M.; Akram, M.A.; Janjua, M.M.; Ahmadlouydarab, M. Nanoparticles enhanced Phase Change Materials (NePCMs)-A Recent Review. *Appl. Therm. Eng.* **2020**, 115305. [CrossRef]
10. Singh, H.; Saini, R.; Saini, J. A review on packed bed solar energy storage systems. *Renew. Sustain. Energy Rev.* **2010**, *14*, 1059–1069. [CrossRef]
11. de Gracia, A.; Cabeza, L.F. Numerical simulation of a PCM packed bed system: a review. *Renew. Sustain. Energy Rev.* **2017**, *69*, 1055–1063. [CrossRef]
12. Hemida, H.; Sabry, M.N.; Abdel-Rahim, A.; Mansour, H. Theoretical analysis of heat transfer in laminar pulsating flow. *Int. J. Heat Mass Transf.* **2002**, *45*, 1767–1780. [CrossRef]
13. Khosravi-Bizhaem, H.; Abbassi, A.; Ravan, A.Z. Heat transfer enhancement and pressure drop by pulsating flow through helically coiled tube: An experimental study. *Appl. Therm. Eng.* **2019**, *160*, 114012. [CrossRef]
14. Naphon, P.; Wiriyasart, S. Experimental study on laminar pulsating flow and heat transfer of nanofluids in micro-fins tube with magnetic fields. *Int. J. Heat Mass Transf.* **2018**, *118*, 297–303. [CrossRef]
15. Cho, H.; Hyun, J.M. Numerical solutions of pulsating flow and heat transfer characteristics in a pipe. *Int. J. Heat Fluid Flow* **1990**, *11*, 321–330. [CrossRef]
16. Wang, Y.; He, Y.L.; Yang, W.W.; Cheng, Z.D. Numerical analysis of flow resistance and heat transfer in a channel with delta winglets under laminar pulsating flow. *Int. J. Heat Mass Transf.* **2015**, *82*, 51–65. [CrossRef]
17. Selimefendigil, F.; Oztop, H.F. Control of laminar pulsating flow and heat transfer in backward-facing step by using a square obstacle. *J. Heat Transf.* **2014**, *136*, 081701. [CrossRef]
18. Al-Habahbeh, O.; Al-Saqqa, M.; Safi, M.; Khater, T.A. Review of magnetohydrodynamic pump applications. *Alex. Eng. J.* **2016**, *55*, 1347–1358. [CrossRef]
19. Kabeel, A.; El-Said, E.M.; Dafea, S. A review of magnetic field effects on flow and heat transfer in liquids: Present status and future potential for studies and applications. *Renew. Sustain. Energy Rev.* **2015**, *45*, 830–837. [CrossRef]
20. M'hamed, B.; Sidik, N.A.C.; Yazid, M.N.A.W.M.; Mamat, R.; Najafi, G.; Kefayati, G. A review on why researchers apply external magnetic field on nanofluids. *Int. Commun. Heat Mass Transf.* **2016**, *78*, 60–67. [CrossRef]
21. Rudraiah, N.; Barron, R.; Venkatachalappa, M.; Subbaraya, C. Effect of a magnetic field on free convection in a rectangular enclosure. *Int. J. Eng. Sci.* **1995**, *33*, 1075–1084. [CrossRef]
22. Grosan, T.; Revnic, C.; Pop, I.; Ingham, D. Magnetic field and internal heat generation effects on the free convection in a rectangular cavity filled with a porous medium. *Int. J. Heat Mass Transf.* **2009**, *52*, 1525–1533. [CrossRef]

23. Gibanov, N.S.; Sheremet, M.A.; Oztop, H.F.; Abu-Hamdeh, N. Effect of uniform inclined magnetic field on mixed convection in a lid-driven cavity having a horizontal porous layer saturated with a ferrofluid. *Int. J. Heat Mass Transf.* **2017**, *114*, 1086–1097. [CrossRef]
24. Selimefendigil, F.; Öztop, H.F. Effects of local curvature and magnetic field on forced convection in a layered partly porous channel with area expansion. *Int. J. Mech. Sci.* **2020**, *179*, 105696. [CrossRef]
25. Chamkha, A.J.; Jena, S.K.; Mahapatra, S.K. MHD convection of nanofluids: A review. *J. Nanofluids* **2015**, *4*, 271–292. [CrossRef]
26. Sheikholeslami, M.; Rokni, H.B. Simulation of nanofluid heat transfer in presence of magnetic field: A review. *Int. J. Heat Mass Transf.* **2017**, *115*, 1203–1233. [CrossRef]
27. Wang, G.; Zhang, Z.; Wang, R.; Zhu, Z. A review on heat transfer of nanofluids by applied electric field or magnetic field. *Nanomaterials* **2020**, *10*, 2386. [CrossRef] [PubMed]
28. Hayat, T.; Sajjad, R.; Muhammad, T.; Alsaedi, A.; Ellahi, R. On MHD nonlinear stretching flow of Powell–Eyring nanomaterial. *Results Phys.* **2017**, *7*, 535–543. [CrossRef]
29. Tian, X.Y.; Li, B.W.; Hu, Z.M. Convective stagnation point flow of a MHD non-Newtonian nanofluid towards a stretching plate. *Int. J. Heat Mass Transf.* **2018**, *127*, 768–780. [CrossRef]
30. Hsiao, K.L. Combined electrical MHD heat transfer thermal extrusion system using Maxwell fluid with radiative and viscous dissipation effects. *Appl. Therm. Eng.* **2017**, *112*, 1281–1288. [CrossRef]
31. Hsiao, K.L. Micropolar nanofluid flow with MHD and viscous dissipation effects towards a stretching sheet with multimedia feature. *Int. J. Heat Mass Transf.* **2017**, *112*, 983–990. [CrossRef]
32. Selimefendigil, F.; Öztop, H.F. MHD mixed convection and entropy generation of power law fluids in a cavity with a partial heater under the effect of a rotating cylinder. *Int. J. Heat Mass Transf.* **2016**, *98*, 40–51. [CrossRef]
33. Kefayati, G.R. Simulation of heat transfer and entropy generation of MHD natural convection of non-Newtonian nanofluid in an enclosure. *Int. J. Heat Mass Transf.* **2016**, *92*, 1066–1089. [CrossRef]
34. Shah, T.R.; Ali, H.M. Applications of hybrid nanofluids in solar energy, practical limitations and challenges: a critical review. *Sol. Energy* **2019**, *183*, 173–203. [CrossRef]
35. Borode, A.; Ahmed, N.; Olubambi, P. A review of solar collectors using carbon-based nanofluids. *J. Clean. Prod.* **2019**, *241*, 118311. [CrossRef]
36. Kakaç, S.; Pramuanjaroenkij, A. Review of convective heat transfer enhancement with nanofluids. *Int. J. Heat Mass Transf.* **2009**, *52*, 3187–3196. [CrossRef]
37. Sajid, M.U.; Ali, H.M. Recent advances in application of nanofluids in heat transfer devices: A critical review. *Renew. Sustain. Energy Rev.* **2019**, *103*, 556–592. [CrossRef]
38. Yadav, C.; Sahoo, R.R. Effect of nano-enhanced PCM on the thermal performance of a designed cylindrical thermal energy storage system. *Exp. Heat Transf.* **2021**, *34*, 356–375. [CrossRef]
39. Mousavi, S.; Siavashi, M.; Heyhat, M.M. Numerical melting performance analysis of a cylindrical thermal energy storage unit using nano-enhanced PCM and multiple horizontal fins. *Numer. Heat Transf. Part A Appl.* **2019**, *75*, 560–577. [CrossRef]
40. Khan, M.M.A.; Ibrahim, N.I.; Mahbubul, I.; Ali, H.M.; Saidur, R.; Al-Sulaiman, F.A. Evaluation of solar collector designs with integrated latent heat thermal energy storage: a review. *Sol. Energy* **2018**, *166*, 334–350. [CrossRef]
41. Jamil, F.; Ali, H.M.; Nasir, M.A.; Karahan, M.; Janjua, M.; Naseer, A.; Ejaz, A.; Pasha, R.A. Evaluation of photovoltaic panels using different nano phase change material and a concise comparison: An experimental study. *Renew. Energy* **2021**, *169*, 1265–1279. [CrossRef]
42. Dinh, M.T.; Tlili, I.; Dara, R.N.; Shafee, A.; Al-Jahmany, Y.Y.Y.; Nguyen-Thoi, T. Nanomaterial treatment due to imposing MHD flow considering melting surface heat transfer. *Phys. A Stat. Mech. Appl.* **2020**, *541*, 123036. [CrossRef]
43. Kohyani, M.T.; Ghasemi, B.; Raisi, A.; Aminossadati, S. Melting of cyclohexane–Cu nano-phase change material (nano-PCM) in porous medium under magnetic field. *J. Taiwan Inst. Chem. Eng.* **2017**, *77*, 142–151. [CrossRef]
44. Selimefendigil, F.; Öztop, H.F. Impacts of rotating surface and oriented magnetic field on mixed convection and melting behavior of CNT-water nanouid in a horizontal annulus. *Int. Commun. Heat Mass Transf.* **2021**, *120*, 104935. [CrossRef]
45. Sheikholeslami, M. Solidification of NEPCM under the effect of magnetic field in a porous thermal energy storage enclosure using CuO nanoparticles. *J. Mol. Liq.* **2018**, *263*, 303–315. [CrossRef]
46. Hashemi-Tilehnoee, M.; Dogonchi, A.; Seyyedi, S.M.; Sharifpur, M. Magneto-fluid dynamic and second law analysis in a hot porous cavity filled by nanofluid and nano-encapsulated phase change material suspension with different layout of cooling channels. *J. Energy Storage* **2020**, *31*, 101720. [CrossRef]
47. Selimefendigil, F.; Öztop, H.F. Impacts of magnetic field and hybrid nanoparticles in the heat transfer fluid on the thermal performance of phase change material installed energy storage system and predictive modeling with artificial neural networks. *J. Energy Storage* **2020**, *32*, 101793. [CrossRef]
48. Sheikholeslami, M.; Rashidi, M.; Ganji, D. Effect of non-uniform magnetic field on forced convection heat transfer of Fe3O4–water nanofluid. *Comput. Methods Appl. Mech. Eng.* **2015**, *294*, 299–312. [CrossRef]
49. Mehryan, S.; Izadi, M.; Chamkha, A.J.; Sheremet, M.A. Natural convection and entropy generation of a ferrofluid in a square enclosure under the effect of a horizontal periodic magnetic field. *J. Mol. Liq.* **2018**, *263*, 510–525. [CrossRef]
50. Selimefendigil, F.; Öztop, H.F. MHD Pulsating forced convection of nanofluid over parallel plates with blocks in a channel. *Int. J. Mech. Sci.* **2019**, *157*, 726–740. [CrossRef]

51. Urmi, W.; Rahman, M.; Hamzah, W. An experimental investigation on the thermophysical properties of 40% ethylene glycol based TiO2-Al2O3 hybrid nanofluids. *Int. Commun. Heat Mass Transf.* **2020**, *116*, 104663. [CrossRef]
52. Nield, D.; Bejan, A. *Convection in Porous Media, in Convection Heat Transfer*; John Wiley & Sons, Inc.: Hoboken, NJ, USA, 2013.
53. COMSOL. *Comsol User's Guide*; COMSOL: Stockholm, Sweden, 2018.
54. Wakao, N.; Kaguei, S.; Funazkri, T. Effect of fluid dispersion coefficients on particle-to-fluid heat transfer coefficients in packed beds: correlation of Nusselt numbers. *Chem. Eng. Sci.* **1979**, *34*, 325–336. [CrossRef]
55. Ghasemi, B.; Aminossadati, S.; Raisi, A. Magnetic field effect on natural convection in a nanofluid-filled square enclosure. *Int. J. Therm. Sci.* **2011**, *50*, 1748–1756. [CrossRef]
56. Wolff, F.; Viskanta, R. Solidification of a pure metal at a vertical wall in the presence of liquid superheat. *Int. J. Heat Mass Transf.* **1988**, *31*, 1735–1744. [CrossRef]